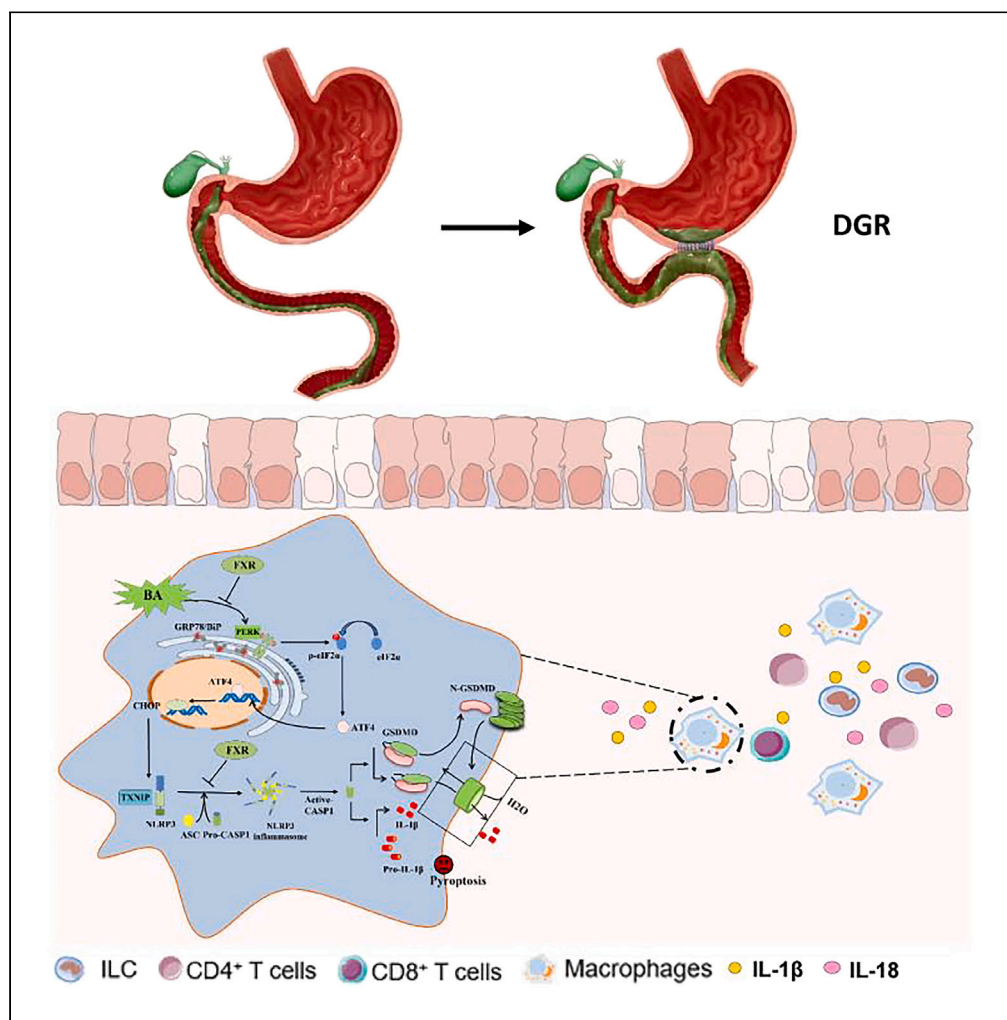


## Article

## FXR controls duodenogastric reflux-induced gastric inflammation through negatively regulating ER stress-associated TNXIP/NLRP3 inflammasome



Junhui Yu, Chenye Zhao, Pengwei Zhao, Mingchao Mu, Xiaopeng Li, Jianbao Zheng, Xuejun Sun

sunxy@mail.xjtu.edu.cn

## Highlights

DGR induces TNXIP/NLRP3 inflammasome activation and triggers pyroptosis in gastric mucosa

FXR antagonizes DGR-induced PERK/eIF2 $\alpha$ /CHOP pathway and reduces TNXIP and NLRP3 level

FXR retards NLRP3 inflammasome activation by physically binding with NLRP3 and caspase-1

## Article

## FXR controls duodenogastric reflux-induced gastric inflammation through negatively regulating ER stress-associated TXNIP/NLRP3 inflammasome

Junhui Yu,<sup>1,2</sup> Chenye Zhao,<sup>1,2</sup> Pengwei Zhao,<sup>1</sup> Mingchao Mu,<sup>1</sup> Xiaopeng Li,<sup>1</sup> Jianbao Zheng,<sup>1</sup> and Xuejun Sun<sup>1,3,\*</sup>

## SUMMARY

**Duodenogastric reflux (DGR) is closely associated with gastric inflammation and tumorigenesis; however, the precise mechanism is unclear. Hence, we aim to clarify this molecular mechanism and design an effective therapeutic strategy based on it. The present study found that DGR induced TXNIP/NLRP3 inflammasome activation and triggered pyroptosis in gastric mucosa *in vitro* and *in vivo*, in which endoplasmic reticulum (ER) stress via PERK/eIF2 $\alpha$ /CHOP signaling was involved. Mechanistically, farnesoid X receptor (FXR) antagonized the DGR-induced PERK/eIF2 $\alpha$ /CHOP pathway and reduced TXNIP and NLRP3 expression. Moreover, FXR suppressed NLRP3 inflammasome activation by physically interacting with NLRP3 and caspase-1. Administration of the FXR agonist OCA protected the gastric mucosa from DGR-induced barrier disruption and mucosal inflammation. In conclusion, our study demonstrates the involvement of TXNIP/NLRP3 inflammasome-mediated pyroptosis in DGR-induced gastric inflammation. FXR antagonizes gastric barrier disruption and mucosal inflammation induced by DGR. Restoration of FXR activity may be a therapeutic strategy for DGR-associated gastric tumorigenesis.**

## INTRODUCTION

Gastric cancer (GC) ranks as the third most common human malignancy worldwide, accounting for the second most tumor-related deaths.<sup>1</sup> It is estimated that half of newly diagnosed GC cases occur in China. GC is the third leading malignancy in terms of incidence and tumor-related death in China.<sup>2</sup> Gastric stump cancer (GSC) is widely recognized as a distinct subtype of GC that develops in the remnant gastric mucosa following gastric resections for both benign disease and cancer. The incidence of GSC is continuously increasing, accounting for 1%–8% of all GC cases. GSC is closely associated with duodenogastric reflux (DGR) due to changes in gastrointestinal anatomy after gastric excision.<sup>3</sup> The anastomotic site after Billroth II gastrectomy is more susceptible to developing GSC than that after Billroth I gastrectomy. The persistent exposure of the anastomotic site to DGR results in gastric mucosal barrier injury and inflammation and eventually progresses to gastric pre-malignant and malignant lesions.<sup>4,5</sup> Among the duodenal components of DGR, bile acids, especially deoxycholic acid (DCA), are widely considered carcinogens in gastrointestinal tumors.<sup>6</sup> Bile acids trigger inflammatory responses in various pathophysiological processes and diseases, including cholestasis and colitis.<sup>7,8</sup> However, the molecular mechanism underlying the initiation of gastric mucosal inflammation by DGR is obscure.

The innate immune system has the capacity to recognize microbes or endogenous molecules, known as damage-associated molecular patterns (DAMPs) or pathogen-associated molecular patterns (PAMPs), via host pattern recognition receptors (PRRs).<sup>9</sup> Activation of PRRs can initiate inflammatory signal transduction cascades to trigger inflammation. The NLRP3 inflammasome, the most fully comprehensively characterized inflammasome, is triggered by multiple PAMPs or DAMPs in the inflammatory response.<sup>10</sup> Upon ligand sensing, NLRP3 and ASC form a platform for recruiting and activating caspase-1.<sup>11</sup> Active caspase-1 catalyzes the maturation and release of IL-1 $\beta$ /18 and drives pyroptosis via the cleavage of gasdermin D (GSDMD).<sup>12</sup> Emerging evidence indicates that the NLRP3 inflammasome plays a key role in the pathogenesis of various metabolic disorders and cancers.<sup>13,14</sup>

Disruption of endoplasmic reticulum (ER) function elicits the unfolded protein response (UPR) to reestablish ER homeostasis and maintain cell survival, a process termed ER stress.<sup>15</sup> The UPR involves three transmembrane sensors: PERK, ATF6, and IRE1. Failure of the UPR to alleviate ER stress results in programmed cell death, including apoptosis, autophagy, and pyroptosis, notably via CHOP, whose expression is highly induced by ER stress.<sup>16,17</sup> Thioredoxin-interacting protein (TXNIP), a negative regulator of redox stress, can be rapidly induced by PERK and IRE1 signaling upon ER stress.<sup>18</sup> The elevated TXNIP subsequently elicits NLRP3 inflammasome activation. TXNIP plays a central role linking ER stress and the NLRP3 inflammasome.<sup>19,20</sup> However, the role of the ER stress-mediated TXNIP/NLRP3 inflammasome in DGR-induced gastric mucosal inflammation remains unclear.

<sup>1</sup>Department of General Surgery, First Affiliated Hospital of Xi'an Jiaotong University, Xi'an 710061, P.R. China

<sup>2</sup>These authors contributed equally

<sup>3</sup>Lead contact

\*Correspondence: [sunxy@mail.xjtu.edu.cn](mailto:sunxy@mail.xjtu.edu.cn)

<https://doi.org/10.1016/j.isci.2024.109118>



Farnesoid X receptor (FXR) belongs to the nuclear receptor superfamily and exhibits a high affinity for bile acids.<sup>21</sup> FXR primarily maintains bile acid homeostasis by regulating the transcription of diverse genes related to hepatic bile acid synthesis and enterohepatic circulation.<sup>22</sup> Ligand-mediated FXR activation in the liver exerts multiple protective effects against metabolic disorders, including diabetes,<sup>23</sup> cholestasis,<sup>24</sup> and nonalcoholic fatty liver disease,<sup>25</sup> and several FXR ligands have been evaluated in clinical trials. Our previous study indicated that long exposure of the gastric mucosa to bile acids stimulates FXR levels.<sup>26</sup> It is possible that the activation of FXR is a protective mechanism of the gastric mucosa reacting to bile acid-induced inflammatory injury;<sup>27</sup> however, the precise mechanism is still unknown. Hence, we aim to clarify this molecular mechanism and design an effective therapeutic strategy.

## RESULTS

### DGR induced gastric barrier disruption and mucosal inflammation

To mimic the influence of DGR on gastric mucosal barrier injury and inflammation, a C57BL/6 mouse model of DGR was established by performing gastrojejunostomy (GJ, [Figure 1A](#)). We first detected the content of asymmetric dimethylarginine (ADMA) in gastric tissues.<sup>28</sup> The results showed that ADMA increased in the GJ group in a time-dependent manner, which reflected obvious damage to the gastric barrier ([Figure 1B](#)). We then determined the detrimental influence of DGR on gastric barrier function by assessing transepithelial electrical resistance (TER). TER decreased in the GJ group, and a longer DGR period caused a greater decrease in TER ([Figure 1C](#)). The dysregulation of tight junctions reflects increased gastric permeability, which is associated with the risk of malignancies.<sup>29</sup> We found that the protein levels of ZO-1, occludin, and claudin-5 were decreased upon DGR exposure in a time-dependent manner ([Figure 1D](#)).

Gastric mucosal inflammation triggered by DGR was evaluated by H&E staining. A striking rise in chronic inflammation was observed in the GJ group, and the severity degree increased with the time since DGR exposure ([Figure 1E](#)). Moreover, three proinflammatory cytokines, IL-6, IL-1 $\beta$ , and TNF- $\alpha$ , were consistently elevated in the GJ group, and a longer DGR exposure led to a more marked elevation of these cytokines ([Figures 1F–1H](#)), indicating that an excessive inflammatory response occurred after DGR exposure.

An *in vitro* DGR model was established by treating normal GES-1 and RGM-1 gastric epithelial cells with DCA in intervals. Consistently, treatment of GES-1 and RGM-1 cells with DCA led to a decrease in the protein levels of ZO-1, occludin, and claudin-5 ([Figures S1A and S1B](#)). Collectively, these data indicated that DGR induced gastric barrier disruption and mucosal inflammation.

### DGR induced TXNIP/NLRP3 inflammasome activation and triggered pyroptosis

To explore the molecular mechanism of DGR-induced gastric mucosal inflammation, RNA sequencing analysis of PMA-differentiated U-937 macrophages with DCA and the control cells was performed. Compared with the control group, 7538 transcripts were differentially expressed in the DGR group, of which 3654 were downregulated and 3498 were upregulated ([Figure 2A](#)). KEGG enrichment analysis suggested that the differentially expressed genes after DGR were enriched in apoptosis and inflammatory signaling pathways, such as lysosome, chemokine signaling pathway, p53 signaling pathway, NOD-like receptor signaling pathway, Toll-like receptor signaling pathway, necroptosis, and NF- $\kappa$ B signaling pathway ([Figure 2B](#)). These data verify that DGR induces cell death and triggers inflammation. To further investigate the mechanism, heatmaps of differentially expressed genes associated with pyroptosis were generated by quantitative real-time PCR ([Figure 2C](#)). The obvious gene changes confirmed that DGR was able to activate pyroptosis pathways.

Pyroptosis can be triggered by the TXNIP/NLRP3 inflammasome in inflammatory processes and responses.<sup>30,31</sup> Herein, the activation of the TXNIP/NLRP3 inflammasome in DGR-induced gastric inflammation was evaluated. We treated PMA-differentiated U-937 and RAW 264.7 macrophages with DCA. DCA treatment dramatically promoted lactate dehydrogenase (LDH) release and inhibited cell viability in a time-dependent manner ([Figures S1C and S1D](#)). Moreover, western blotting analysis showed that DGR resulted in an increase in NLRP3 and TXNIP levels as well as active caspase-1, IL-1 $\beta$ , and IL-18 ([Figures 3A–3C](#)). No alteration was observed in the ASC level. The elevation of NLRP3 was further confirmed by immunofluorescence (IF) staining ([Figure 3D](#)). GSDMD is the executor of pyroptosis,<sup>12</sup> and we observed an induction of the GSDMD-N fragment in the DGR model *in vitro* ([Figure 3E](#)). To clarify that pyroptosis was one of the major forms of cell death triggered by DGR, we knocked down GSDMD to abrogate pyroptosis in macrophages. As expected, depletion of GSDMD dramatically ameliorated the effect of DCA on LDH release and cell viability ([Figures 3F and 3G](#)). Collectively, these data indicated that TXNIP/NLRP3 inflammasome-mediated pyroptosis is involved in DGR-triggered gastric mucosal inflammation.

### DGR induced TXNIP/NLRP3 inflammasome activation by modulating the PERK/eIF2 $\alpha$ /CHOP pathway

A previous study indicated that bile acids induced by high-fat feeding can impair the intestinal barrier by inducing ER stress.<sup>32</sup> ER stress plays an important role in TXNIP/NLRP3 inflammasome activation.<sup>16,17</sup> Thus, we speculate that ER stress might participate in the regulatory effect of DGR on the TXNIP/NLRP3 inflammasome. We detected the expression of pivotal molecules of the three branches of the UPR (PERK, ATF6, and IRE1 branches). Interestingly, elevations in p-PERK, p-eIF2 $\alpha$ , and CHOP levels were observed in the DGR model *in vivo* and *in vitro* ([Figures 4A and 4B](#)). GRP78 displayed parallel levels ([Figures 4A and 4B](#)). However, DGR did not affect the levels of ATF6 and IRE1/XBP1 branches ([Figures S2A and S2B](#)).

To further confirm the involvement of the PERK/eIF2 $\alpha$ /CHOP pathway in DGR-mediated TXNIP/NLRP3 inflammasome activation, we knocked down PERK or CHOP and analyzed its effect on the TXNIP/NLRP3 inflammasome. As expected, PERK depletion abrogated the inductive effect of DGR on NLRP3, TXNIP, and CHOP ([Figure 4C](#)). Similar results were achieved by CHOP depletion ([Figure 4D](#)). Collectively, these data revealed that DGR induced TXNIP/NLRP3 inflammasome activation by modulating the PERK/eIF2 $\alpha$ /CHOP pathway.

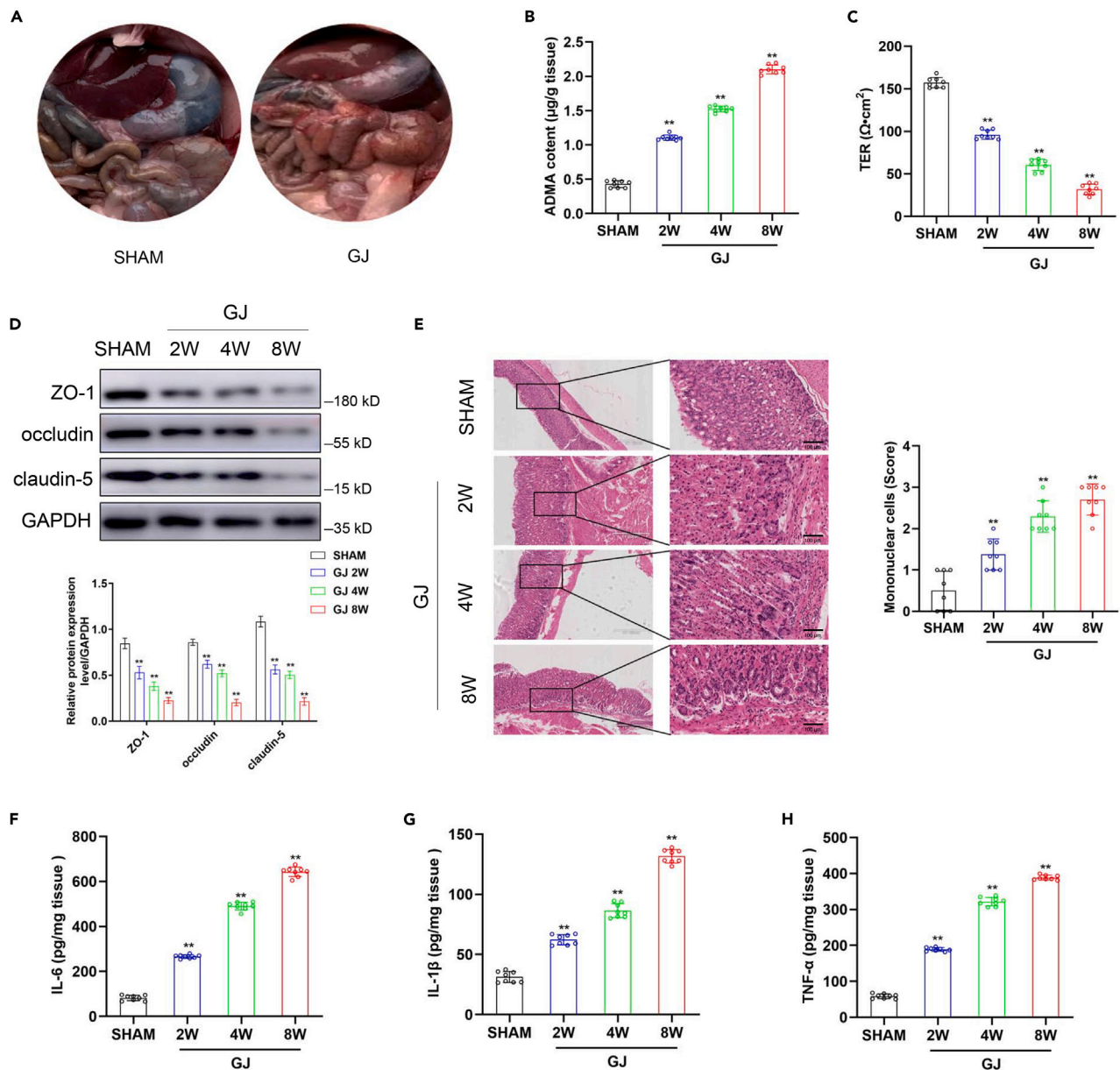


**Figure 1. DGR induced gastric barrier disruption and mucosal inflammation**

(A) C57BL/6 mice model of DGR was established by performing gastrojejunostomy (GJ). The representative images of the sham and GJ operations. (B and C) The integrity of the gastric barrier was evaluated with the tissue ADMA (B) levels and TER (C). (D) The levels of tight junction proteins in gastric mucosa from GJ group at 2, 4, and 8 weeks by western blotting analysis (up panel: gel bands; down panel: quantitative analysis of these proteins). (E) The histopathological damage after DGR exposure estimated with the H&E staining (left panel) and the score of mononuclear cell infiltration (right panel). (F–H) The release of tissue IL-6 (F), IL-1 $\beta$  (G), and TNF- $\alpha$  (H) in gastric mucosa from GJ group at 2, 4, and 8 weeks was measured by ELISA. All data are the mean  $\pm$  SD of three independent experiments. \* $p < 0.05$ , \*\* $p < 0.01$  (one-way ANOVA).

### FXR antagonizes the DGR-induced PERK/eIF2 $\alpha$ /CHOP pathway and reduces TXNIP and NLRP3 expression

FXR activation has protective effects on liver injury by repressing the NLRP3 inflammasome.<sup>33</sup> Herein, we sought to determine the role of FXR in DGR-induced TXNIP/NLRP3 inflammasome activation via FXR loss- or gain-of-function experiments. Intriguingly, RAW264.7 cells with FXR depletion were more prone to the activation of caspase-1 and the maturation of IL-1 $\beta$ /IL-18 in the DGR model *in vitro* (Figure 5A). Consistently, enhancing FXR expression or FXR activation by obeticholic acid (OCA) disrupted the induction of caspase-1 activation and IL-1 $\beta$ /IL-18 maturation (Figures 5B and 5C). The IL-1 $\beta$  levels detected by ELISA further corroborated the negative regulatory effect of FXR on DGR-induced

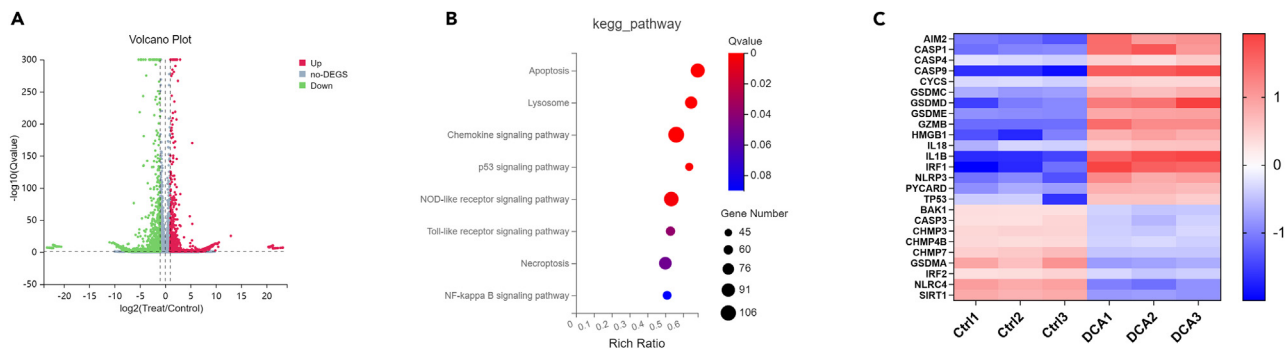


**Figure 2. RNA sequencing analysis of PMA-differentiated U-937 macrophages with DCA and the control cells**

(A) Volcano plots of DGR and control treatments.

(B) Bubble diagram about KEGG enrichment analysis of DGR and control treatments.

(C) Differential gene expression heatmaps of identified genes involved in pyroptosis of DGR and control treatments.

TXNIP/NLRP3 inflammasome activation (Figures 5D and 5E). Modulating FXR expression alone did not affect the levels of the members of the TXNIP/NLRP3 inflammasome (Figures 5A and 5B). However, upon DGR exposure, FXR depletion enhanced the protein levels of TXNIP and NLRP3 (Figure 5A). Conversely, overexpression of FXR or treatment with OCA alleviated the inducing effect of DGR on TXNIP and NLRP3 (Figures 5B and 5C).

We then evaluated the involvement of ER stress in the negative regulation of FXR on TXNIP/NLRP3 inflammasome activation. Depletion of FXR dramatically accelerated the elevation of p-PERK, eIF2 $\alpha$ , CHOP, and GRP78 levels induced by DGR *in vitro* (Figure 5F). Conversely, FXR overexpression or OCA treatment attenuated this induction by DGR (Figures 5G and 5H). Overall, these data indicated that FXR antagonizes DGR-induced NLRP3 inflammasome activation by regulating ER stress.

### FXR antagonizes DGR-induced TXNIP/NLRP3 inflammasome activation through its interaction with NLRP3 and CASP-1

We next assumed that FXR might physically interact with members of the NLRP3 inflammasome to repress its activation. The results from IF staining supported the colocalization of FXR and NLRP3 and caspase-1 (Figures 6A and 6B). Co-immunoprecipitation assays were further conducted to investigate the binding of FXR to NLRP3 and caspase-1. Immunoprecipitation of FXR verified that FXR bound to NLRP3 and caspase-1 in RAW264.7 macrophages (Figure 6C). DCA alone slightly repressed the interactions of FXR with NLRP3 and caspase-1; however, silencing FXR expression dramatically impaired these interactions (Figure 6D). Conversely, FXR activation by OCA strengthened the interactions among these proteins (Figure 6E). These data provide evidence that FXR might suppress TXNIP/NLRP3 inflammasome activation by hindering inflammasome assembly by interacting with NLRP3 and caspase-1.

### The FXR agonist OCA protected against DGR-induced gastric barrier disruption and mucosal inflammation

The results mentioned previously indicated that restoration of FXR by its ligand might represent a promising therapeutic approach for DGR-induced gastric inflammation. Hence, different doses of OCA were first administered before establishing the GJ model *in vivo*.<sup>34</sup> The results from H&E staining revealed that OCA ameliorates gastric inflammation progression induced by DGR in a dose-dependent manner (Figure 7C). Moreover, the decline in ADMA and TER by DGR was abrogated upon OCA treatment (Figure 7A). The recovery of tight junction proteins further confirmed the beneficial effect of OCA on gastric barrier disruption (Figure 7B). The beneficial pharmacological effect of OCA was further confirmed in a DGR model *in vitro*. Treatment with OCA attenuated the release of LDH (Figure 7D) and recovered cell viability (Figure 7E). Collectively, we confirmed that OCA could protect against DGR-induced gastric barrier disruption and mucosal inflammation.

### The FXR agonist OCA protected against DGR-induced TXNIP/NLRP3 inflammasome activation

We further sought to explore the effect of OCA on DGR-induced TXNIP/NLRP3 inflammasome activation. CY-09, a specific inhibitor of the NLRP3 inflammasome, was administered to the DGR model *in vivo* as a positive control. The elevation of IL-6 and IL-1 $\beta$  was hindered by OCA or CY-09 treatment (Figures 8A and 8B). However, OCA or CY-09 treatment did not affect the level of TNF- $\alpha$  (Figure 8C). Next, the components of the TXNIP/NLRP3 inflammasome were analyzed upon OCA exposure. As expected, OCA or CY-09 administration abolished the induction of TXNIP and NLRP3 by DGR, as well as active caspase-1, IL-1 $\beta$ , and IL-18 (Figure 8D). Moreover, IF staining displayed a similar alteration in NLRP3 upon OCA or CY-09 treatment (Figure 8F). The production of the GSDMD-N fragment induced by DGR was abrogated by OCA or CY-09 treatment (Figure 8E).

To demonstrate that pyroptosis inhibition was involved in the protective mechanism of OCA against gastric inflammation, we knocked down GSDMD in macrophages and treated them with OCA. GSDMD depletion abolished the effect of OCA on cell viability (Figure 8G) and LDH (Figure 8H) in the DGR model *in vitro*. Overall, these data concluded that OCA protected against the DGR-induced TXNIP/NLRP3 inflammasome and pyroptosis.

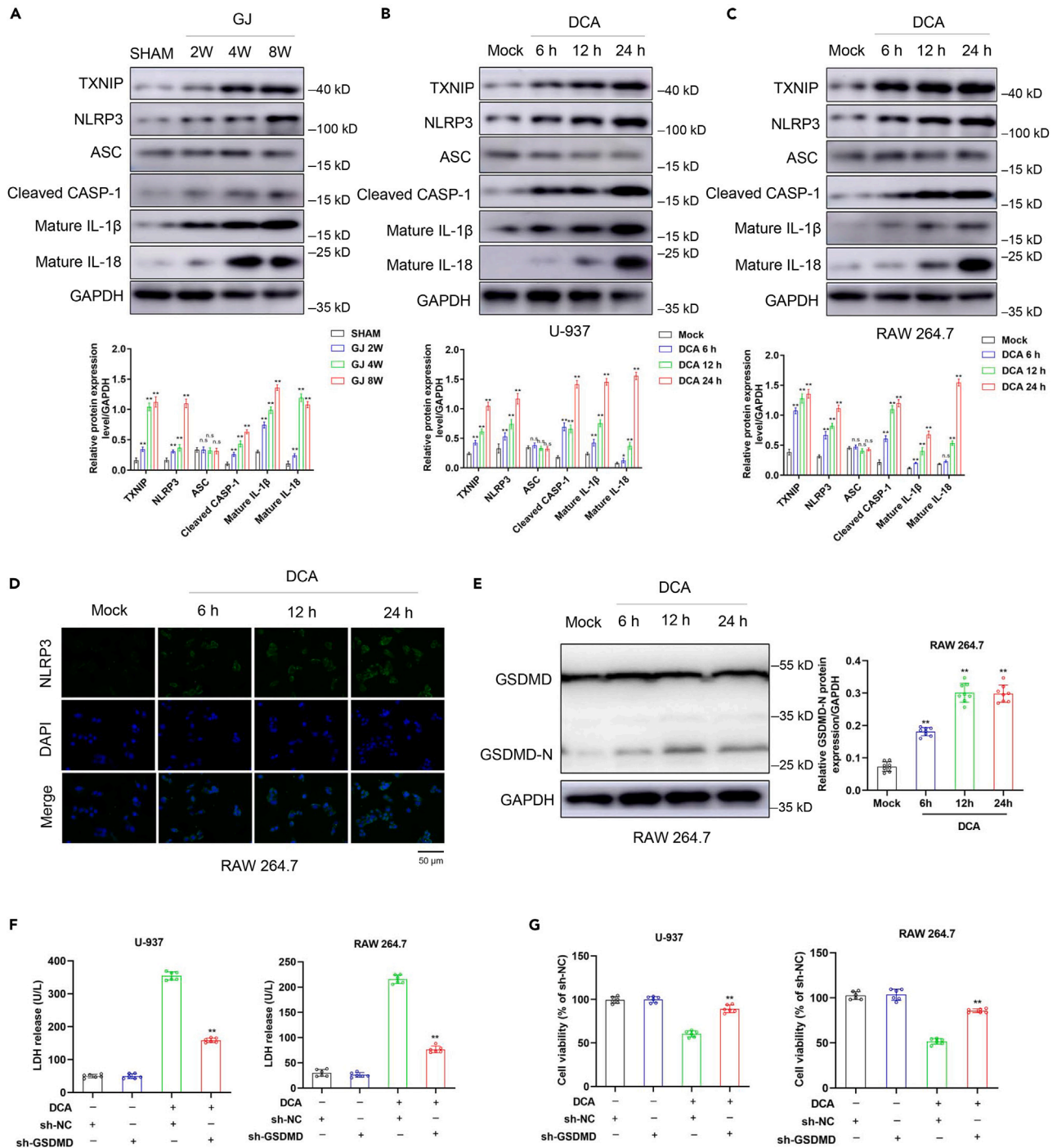


**Figure 3. DGR induced TXNIP/NLRP3 inflammasome activation and triggered pyroptosis**

(A) The levels of TXNIP/NLRP3 inflammasome in gastric mucosa from GJ group at 2, 4, and 8 weeks by western blotting analysis (up panel: gel bands; down panel: quantitative analysis of these proteins).

(B and C) The levels of TXNIP/NLRP3 inflammasome in PMA-differentiated U-937 (B) and RAW 264.7 (C) macrophages treated with 100  $\mu$ M DCA for 6, 12, and 24 h by western blotting analysis (up panel: gel bands; down panel: quantitative analysis of these proteins).

(D) The level of NLRP3 in RAW 264.7 macrophages treated with 100  $\mu$ M DCA for 6, 12, and 24 h by IF staining.

**Figure 3. Continued**

(E) The production of GSDMD-N fragment in RAW 264.7 macrophages treated with 100  $\mu$ M DCA for 6, 12, and 24 h by western blotting analysis (left panel: gel bands; right panel: quantitative analysis of these proteins).

(F) The effect of GSDMD depletion on the release of LDH in PMA-differentiated U-937 and RAW 264.7 by ELISA.

(G) The effect of GSDMD depletion on the cell viability of PMA-differentiated U-937 and RAW 264.7 by CCK8 assay. All data are the mean  $\pm$  SD of three independent experiments. \* $p < 0.05$ , \*\* $p < 0.01$  (one-way ANOVA).

**DISCUSSION**

The incidence of GSC continues to rise due to the wide application of gastrectomy for benign peptic ulcers two or three decades ago.<sup>35</sup> Persistent chronic inflammation in the gastric remnant triggered by DGR contributes to the initiation and progression of GSC.<sup>36</sup> Clinical, animal, and epidemiological investigations have suggested bile acids, the main component of DGR, as the etiology of GSC.<sup>37</sup> Bile acids act as DAMPs that can stimulate both the priming and activation steps of the NLRP3 inflammasome in inflammatory processes.<sup>7,38</sup> One of the notable findings of this study is that we demonstrated for the first time the involvement of the TXNIP/NLRP3 inflammasome in DGR-induced gastric inflammation. We found that TXNIP expression was remarkably elevated in gastric mucosa tissues from the GJ group compared to that in the control group. Consistently, a previous study reported that increased TXNIP expression is observed in *H. pylori*-induced gastritis.<sup>39</sup> Moreover, DGR administration elevated the expression of NLRP3 inflammasome components, including NLRP3, cleaved caspase-1, IL-1 $\beta$ , and IL-18, despite no change in ASC expression. Clinical and experimental studies have demonstrated the contribution of the NLRP3 inflammasome to gastritis, and genetic deletion of NLRP3 and caspase-1 protected mice from severe gastritis.<sup>40</sup> Consistently, activation of TXNIP induces IL-1 $\beta$  mRNA transcription, activates IL-1 $\beta$  production by NLRP3 inflammasome, and mediates ER stress-mediated cell death in diabetes.<sup>18</sup> Thus, targeting TXNIP by pharmacological agents might be a potential therapeutic strategy for ER stress-related human diseases such as gastritis.<sup>41</sup>

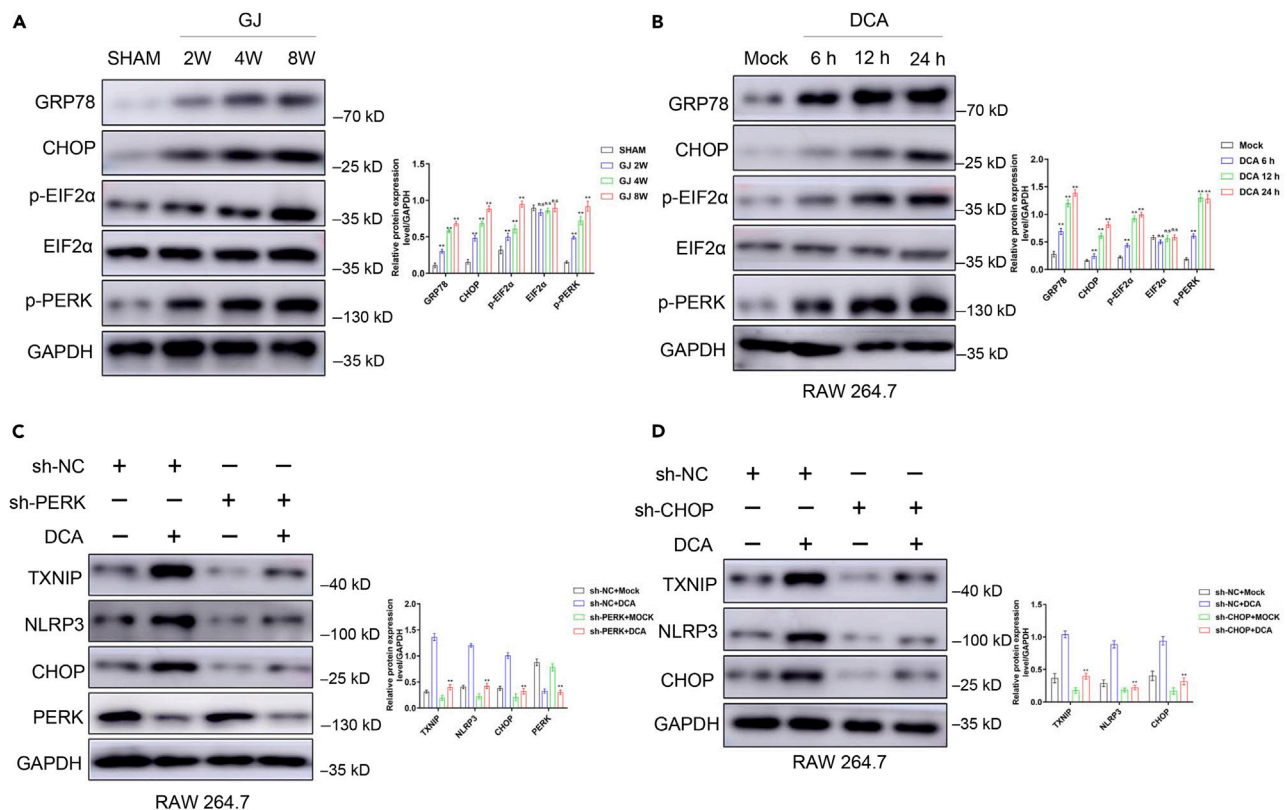


**Figure 4. DGR induced TXNIP/NLRP3 inflammasome activation by modulating PERK/eIF2 $\alpha$ /CHOP pathway**

(A) The levels of PERK/eIF2 $\alpha$ /CHOP branches in gastric mucosa from GJ group at 2, 4, and 8 weeks by western blotting analysis (left panel: gel bands; right panel: quantitative analysis of these proteins).

(B) The levels of PERK/eIF2 $\alpha$ /CHOP branches in RAW 264.7 macrophages treated with 100  $\mu$ M DCA for 6, 12, and 24 h by western blotting analysis (left panel: gel bands; right panel: quantitative analysis of these proteins).

(C and D) The effect of PERK (c) or CHOP (d) knockdown on the levels of PERK/eIF2 $\alpha$ /CHOP branches and TXNIP/NLRP3 inflammasome activation in RAW 264.7 macrophages treated with 100  $\mu$ M DCA for 24 h (left panel: gel bands; right panel: quantitative analysis of these proteins). All data are the mean  $\pm$  SD of three independent experiments. \* $p < 0.05$ , \*\* $p < 0.01$  (one-way ANOVA).

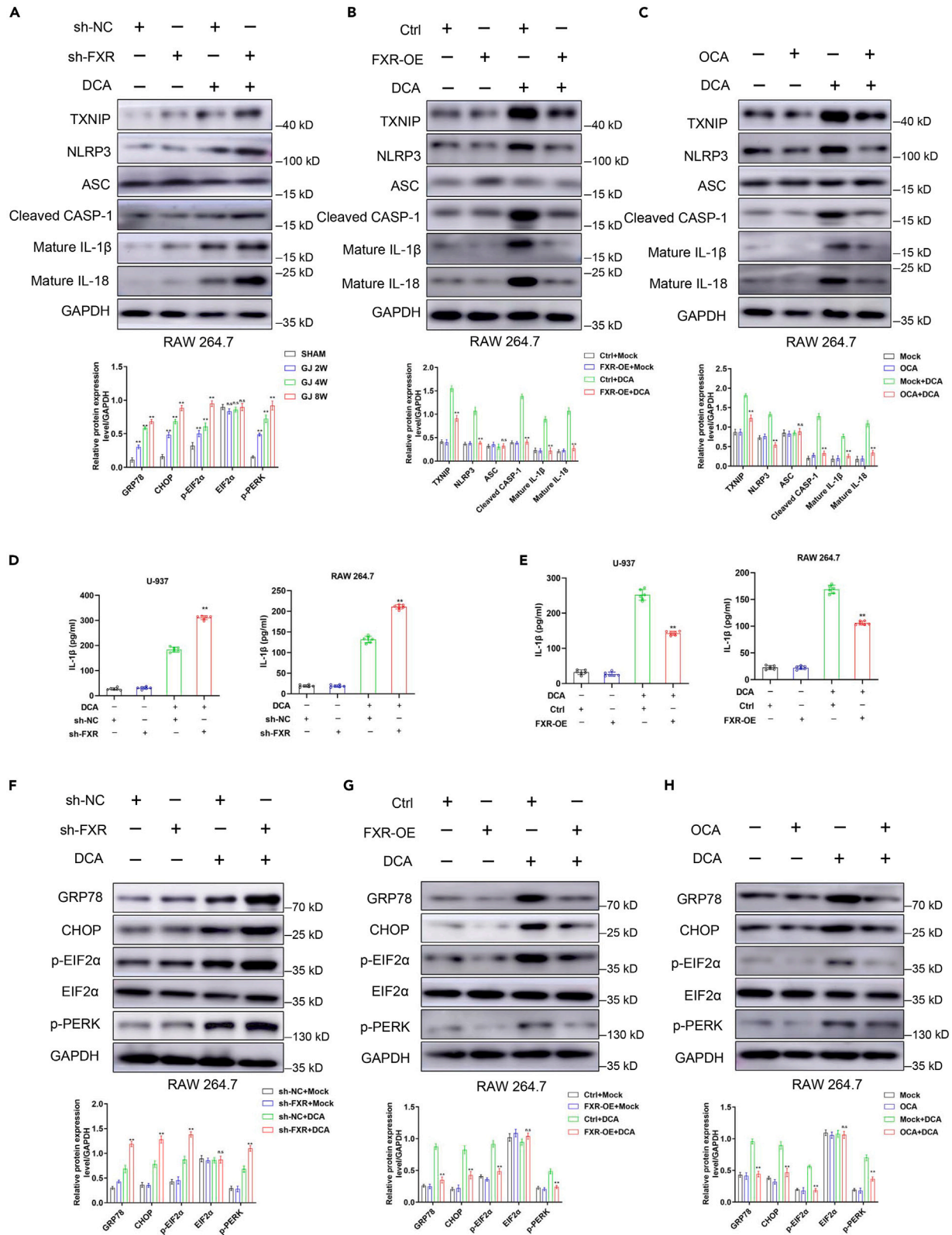


**Figure 5. FXR antagonizes DGR-induced PERK/eIF2 $\alpha$ /CHOP pathway and reduced TXNIP and NLRP3 expression**

(A–C) The effect of FXR knockdown (A), FXR overexpression (B), or FXR agonist OCA (C) on the levels of TXNIP/NLRP3 inflammasome in RAW 264.7 macrophages treated with 100  $\mu$ M DCA for 24 h by western blotting analysis (up panel: gel bands; down panel: quantitative analysis of these proteins). (D and E) The effect of FXR depletion (D) or overexpression (E) on the release of LDH in PMA-differentiated U-937 and RAW 264.7 treated with 100  $\mu$ M DCA for 24 h by ELISA. (F–H) The effect of FXR knockdown (F), FXR overexpression (G), or FXR agonist OCA (H) on the levels of PERK/eIF2 $\alpha$ /CHOP branches in RAW 264.7 macrophages treated with 100  $\mu$ M DCA for 24 h by western blotting analysis (up panel: gel bands; down panel: quantitative analysis of these proteins). All data are the mean  $\pm$  SD of three independent experiments. \*p < 0.05, \*\*p < 0.01 (one-way ANOVA).

Pyroptosis can provoke inflammatory processes by releasing IL-1 $\beta$ /18,<sup>42</sup> which distinguishes it from apoptosis. Herein, in an *in vivo* DGR model, we found that the N-terminal fragment of GSDMD was produced, which verified the occurrence of pyroptosis. By a GSDMD depletion experiment, we confirmed that pyroptosis was one of the major forms of gastric epithelial cell death induced by DGR. The involvement of pyroptosis may explain why DGR induces rapid and severe dysregulation of the gastric mucosal barrier and triggers inflammation.

FXR is a ligand-activated transcription factor involved in the control of bile acid synthesis and enterohepatic circulation.<sup>22</sup> The activation of FXR exerts a powerful anti-inflammatory effect in metabolic disorders.<sup>43</sup> Hepatic FXR activation by OCA is currently used to treat primary biliary cholangitis.<sup>44</sup> Late-stage clinical trials investigating the application of OCA in the treatment of nonalcoholic steatohepatitis are underway.<sup>45</sup> However, the role of FXR in the context of DGR-induced gastric mucosal inflammation remains unclear. Herein, we report an inhibitory effect of FXR on the multilevel regulation of the NLRP3 inflammasome (priming and activation steps) in DGR-induced gastric inflammation. Our data showed that FXR depletion potentiated the inducing effect of DGR on TXNIP and NLRP3 expression in gastric mucosa as well as IL-1 $\beta$  release. Consistently, FXR overexpression or FXR activation by OCA displayed the opposite effect. Intriguingly, we demonstrated that

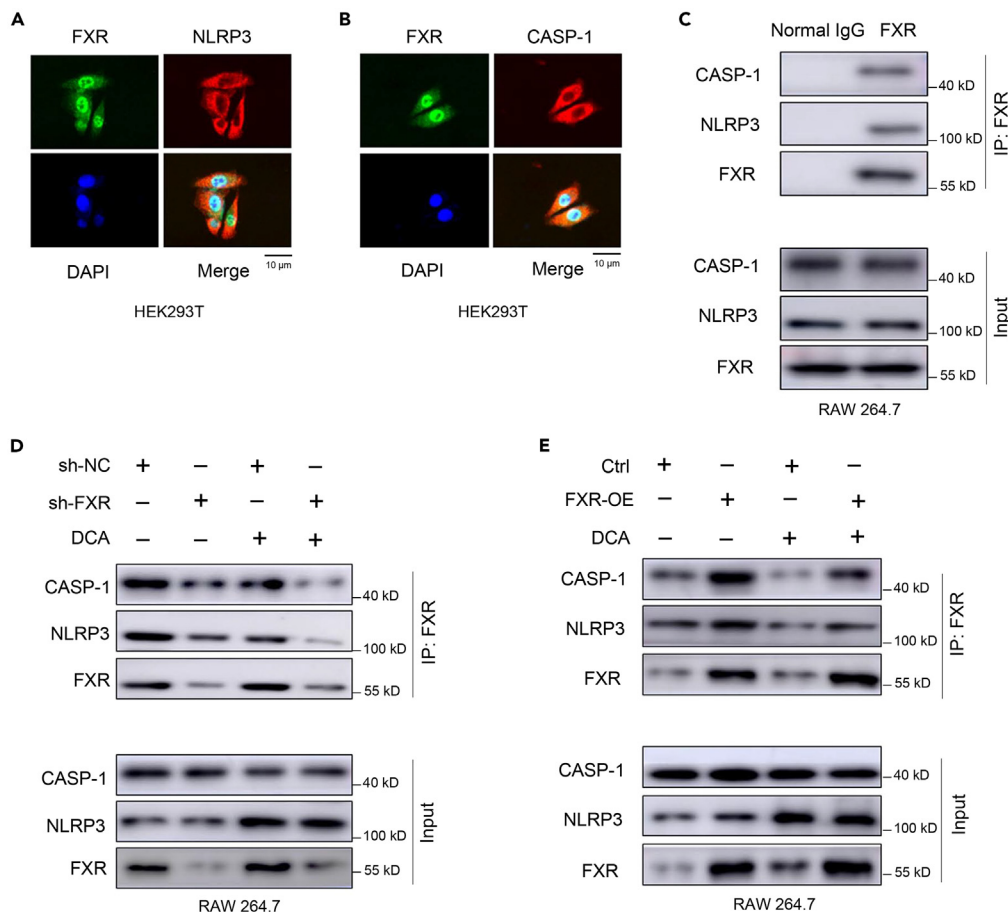


**Figure 6. FXR might physically interact with the members of NLRP3 inflammasome**

(A and B) The co-localization of FXR and NLRP3 (A) and caspase-1 (B) by IF staining (cytoplasm, orange). (C) The bindings of endogenous FXR to NLRP3 and caspase-1 by co-IP assay in RAW 264.7 macrophages. (D and E) The effect of FXR knockdown (D) or FXR agonist OCA (E) on the bindings of FXR to NLRP3 and caspase-1. All data are the mean  $\pm$  SD of three independent experiments.

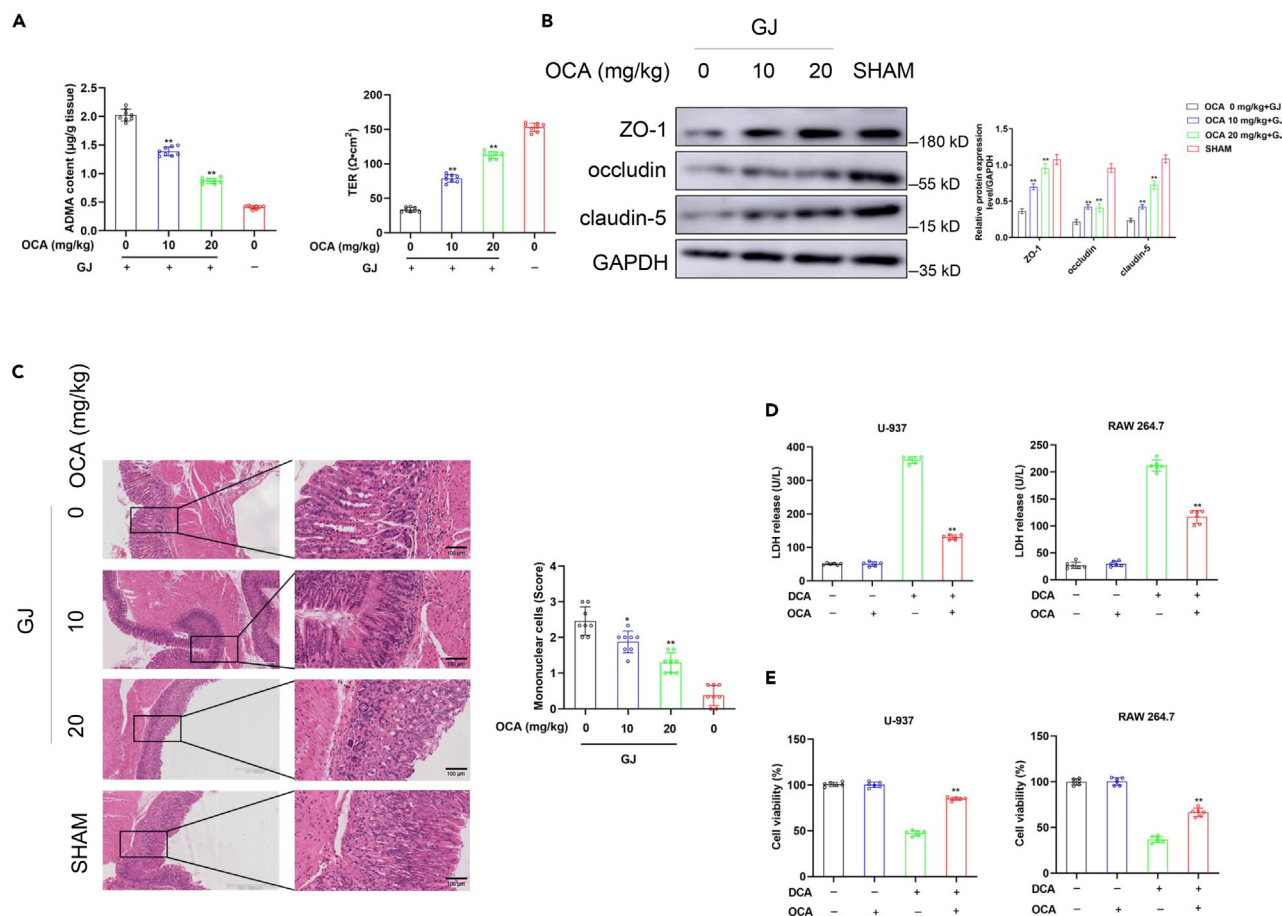


**Figure 7. FXR agonist OCA protected against DGR-induced gastric barrier disruption and mucosal inflammation**

(A) Different doses of OCA were first administered before setting up GJ model *in vivo*. The effect of FXR agonist OCA at different doses on the integrity of the gastric barrier from GJ group at 8 weeks was evaluated with the tissue ADMA levels and TER.

(B) The effect of FXR agonist OCA on the levels of tight junction proteins in gastric mucosa from GJ group at 8 weeks by western blotting analysis (left panel: gel bands; right panel: quantitative analysis of these proteins).

(C) The effect of FXR agonist OCA on the histopathological damage after DGR exposure estimated with the H&E staining (left panel) and the score of mononuclear cell infiltration (right panel).

(D) The effect of FXR agonist OCA on the release of LDH in PMA-differentiated U-937 and RAW 264.7 treated with 100 µM DCA for 24 h by ELISA.

(E) The effect of FXR agonist OCA on the cell viability of PMA-differentiated U-937 and RAW 264.7 by CCK8 assay. All data are the mean ± SD of three independent experiments. \*p < 0.05, \*\*p < 0.01 (one-way ANOVA).

FXR physically interacted with NLRP3 and caspase-1, which might hinder NLRP3 inflammasome assembly and activation (the activation step). A recent study revealed that FXR is upregulated in human gastric IM samples, accompanied by a reduction in IL-1β,<sup>46</sup> confirming the negative regulation of FXR on NLRP3 inflammasome activation. More importantly, OCA administration protected against DGR-induced gastric barrier disruption and mucosal inflammation by alleviating TXNIP/NLRP3 inflammasome activation. Given that OCA in the current research is a non-selective FXR agonist, our finding could not adequately exclude the effect of intestinal FXR signaling activation. Indeed, gut-restricted FXR agonist fexaramine reduces diet-induced body-wide inflammation.<sup>47</sup> Hence, tissues-restricted FXR activation might be the future research in the treatment of these inflammation and metabolic dysfunction.

The gastric mucosa has an abundance of ER, allowing this cell type to serve as a major sensor responding to ER stress.<sup>48</sup> Various pathological signals stimulated by obesity or ethanol in the gastric mucosa can activate the UPR in the ER.<sup>49,50</sup> The ER stress-activated TXNIP/NLRP3 inflammasome contributes to gastric mucosal injury.<sup>39</sup> GRP78 is an ER-specific chaperone involved in the UPR. Our study found increased expression of GRP78 in the gastric mucosa from mice in the GJ group. Elevated expression of GRP78 was previously reported in *Helicobacter*-induced gastric carcinogenesis.<sup>51</sup> PERK is an ER transmembrane UPR sensor protein regulated by GRP78. Active PERK further inhibits translational ribosomal assembly through the phosphorylation of eIF2α. The present study revealed that DGR promoted the phosphorylation of PERK and eIF2α, confirming the activation of ER stress. Elevated ER stress culminates in CHOP-mediated NLRP3 inflammasome activation and pyroptosis.<sup>16,17</sup> As expected, gastric mucosa cells exposed to DGR overexpressed CHOP. Furthermore, CHOP or PERK depletion

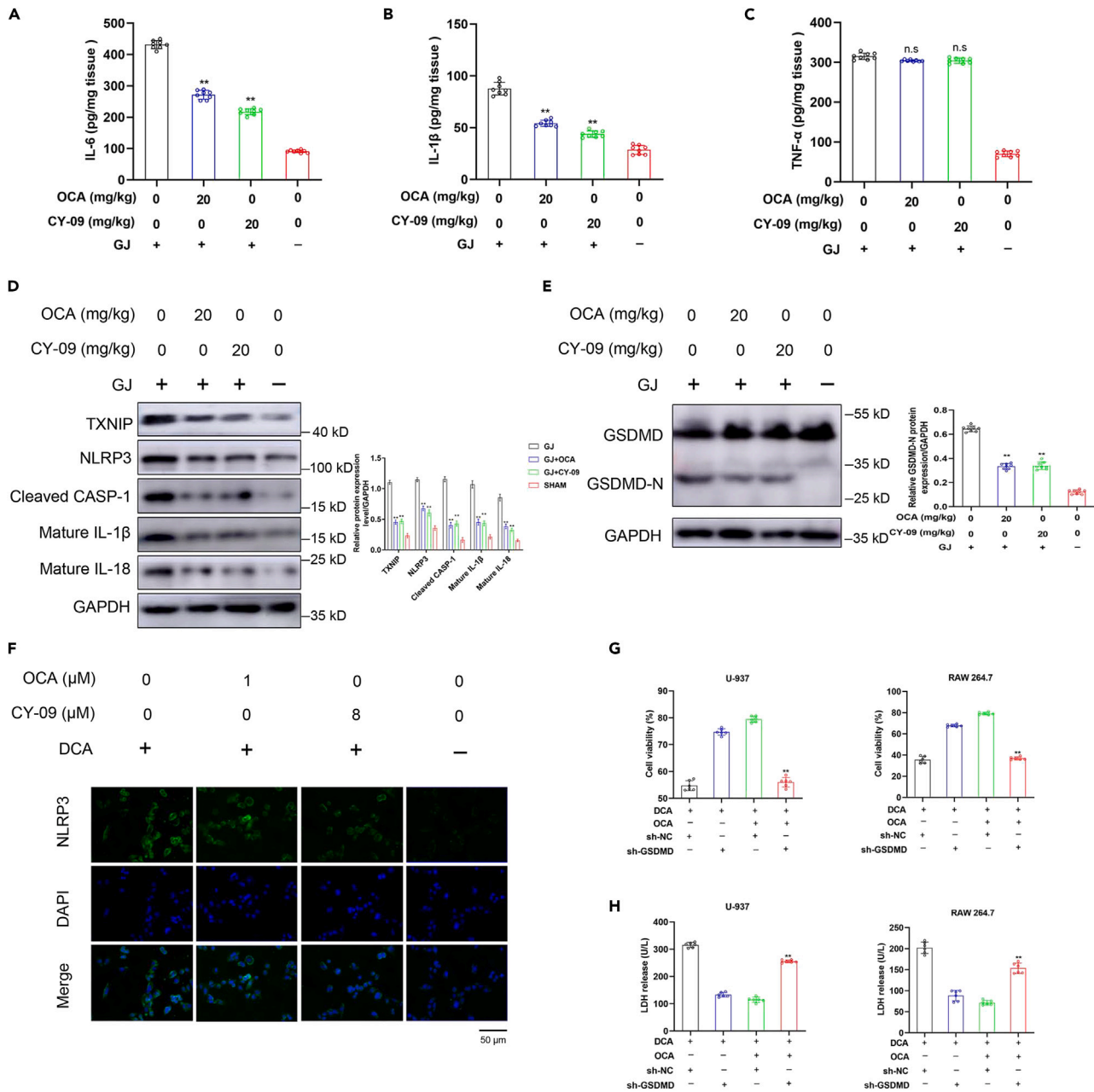


**Figure 8. FXR agonist OCA protected against DGR-induced TXNIP/NLRP3 inflammasome activation**

(A–C) CY-09, a specific inhibitor of NLRP3 inflammasome, was administered to DGR model *in vivo* as positive control. The effect of OCA or CY-09 on the release of tissue IL-6 (A), IL-1 $\beta$  (B), and TNF- $\alpha$  (C) in gastric mucosa from GJ group at 8 weeks by ELISA.

(D) The effect of OCA or CY-09 on the levels of TXNIP/NLRP3 inflammasome gastric mucosa from GJ group at 8 weeks by western blotting analysis (left panel: gel bands; right panel: quantitative analysis of these proteins).

(E) The effect of OCA or CY-09 on the production of GSDMD-N fragment in gastric mucosa from GJ group at 8 weeks by western blotting analysis (left panel: gel bands; right panel: quantitative analysis of these proteins).

(F) The effect of OCA or CY-09 on the level of NLRP3 in RAW 264.7 treated with 100  $\mu$ M DCA for 24 h by IF staining.

(G) The effect of GSDMD depletion on cell viability of PMA-differentiated U-937 and RAW 264.7 treated with 100  $\mu$ M DCA and 1.5  $\mu$ M OCA for 24 h by CCK8 assay.

(H) The effect of GSDMD depletion on the release of LDH in PMA-differentiated U-937 and RAW 264.7 treated with 100  $\mu$ M DCA and 1.5  $\mu$ M OCA for 24 h by ELISA. All data are the mean  $\pm$  SD of three independent experiments. \* $p$  < 0.05, \*\* $p$  < 0.01 (one-way ANOVA).

attenuated the inducing effect of DGR on NLRP3 and TXNIP expression, confirming the central role of ER stress in the TXNIP/NLRP3 inflammasome induced by DGR. An important finding of our study is the identification of FXR as a protective regulator against catastrophic ER stress; our findings show that FXR depletion augmented p-PERK, CHOP, and GRP78 levels upon DGR *in vitro*. Consistently, overexpression of FXR or treatment with OCA alleviated the PERK/eIF2 $\alpha$ /CHOP pathway induced by DGR. In most cases, hepatic ER stress is accompanied by a lowered expression of FXR in aging mice,<sup>52</sup> and multiple FXR agonists have been shown to protect cells from ER stress.<sup>53</sup> FXR activation has a cytoprotective effect in the kidney, which is mediated by suppressing ER stress.<sup>54</sup> Intriguingly, FXR was shown to be decreased upon ER stress, indicating that a feedforward loop might exist between FXR loss and ER stress.<sup>52</sup> Because mitochondrial function is closely linked to ER stress and inflammasome activation, the beneficial effects of FXR on energy metabolism and mitochondrial function<sup>55</sup> may add value to the use of FXR as a therapeutic target for ER stress-associated gastric inflammation in the context of DGR.

In summary, our study demonstrated that DGR induced gastric barrier disruption and mucosal inflammation by activating the TXNIP/NLRP3 inflammasome via ER stress. Our study further revealed the dual regulatory effect of FXR on the NLRP3 inflammasome in DGR-induced gastritis. On the one hand, FXR antagonized the DGR-induced PERK/eIF2 $\alpha$ /CHOP pathway and reduced the expression of TXNIP and NLRP3. On the other hand, FXR physically interacted with NLRP3 and caspase-1, which might hinder NLRP3 inflammasome assembly and activation. In addition, the FXR agonist OCA protected against DGR-induced gastric barrier disruption and mucosal inflammation. Our study might extend the clinical application of OCA in DGR-induced gastric inflammation and tumorigenesis.

### Limitations of the study

A potential limitation of this study is that we have not been able to extend the clinical application of OCA in DGR-induced gastric tumorigenesis *in vivo*. It is still questionable that whether GC occurs in the present GJ models. Further research should be conducted using a carcinogenesis model.

### STAR★METHODS

Detailed methods are provided in the online version of this paper and include the following:

- KEY RESOURCES TABLE
- RESOURCE AVAILABILITY
  - Lead contact
  - Materials availability
  - Data and code availability
- EXPERIMENTAL MODEL AND STUDY PARTICIPANT DETAILS
  - Cell cultures
  - Animal model of DGR
- METHOD DETAILS
  - Lentiviral vectors and transfection
  - CCK-8 assay
  - LDH, IL-1 $\beta$ , IL-6, and TNF- $\alpha$  release assay
  - Measurement of Trans-epithelial electrical resistance (TER)
  - Histopathological analysis
  - Total protein extraction and western blotting
  - RNA isolation and real-time PCR
  - RNA-sequencing
  - Immunofluorescence (IF)
  - Immunoprecipitation (IP) assay
  - Statistical analysis

### SUPPLEMENTAL INFORMATION

Supplemental information can be found online at <https://doi.org/10.1016/j.isci.2024.109118>.

### ACKNOWLEDGMENTS

This work was supported by grants received from the fund for the National Natural Science Foundation of China (grant no. 82002547).

### AUTHOR CONTRIBUTIONS

J.Y. and X.S. contributed to study design and planning, conducting experiments, data analysis, article preparation, and review. C.Z., P.Z., and M.M. contributed to conducting experiments. J.Z. and X.L. contributed to data review and article preparation. X.S. and J.Y. contributed to study design, data analysis, article preparation, and review.

## DECLARATION OF INTERESTS

All authors declare that they have no conflict of interest in the article.

Received: February 22, 2023

Revised: May 15, 2023

Accepted: January 31, 2024

Published: February 6, 2024

## REFERENCES

- Torre, L.A., Bray, F., Siegel, R.L., Ferlay, J., Lortet-Tieulent, J., and Jemal, A. (2015). Global cancer statistics, 2012. *CA. Cancer J. Clin.* **65**, 87–108. <https://10.3322/caac.21262>.
- Chen, W., Zheng, R., Baade, P.D., Zhang, S., Zeng, H., Bray, F., Jemal, A., Yu, X.Q., and He, J. (2016). Cancer statistics in China, 2015. *CA. Cancer J. Clin.* **66**, 115–132. <https://10.3322/caac.21338>.
- Păduraru, D.N., Nica, A., Ion, D., Handaric, M., and Andronic, O. (2016). Considerations on risk factors correlated to the occurrence of gastric stump cancer. *J. Med. Life* **9**, 130–136.
- In Choi, C., Baek, D.H., Lee, S.H., Hwang, S.H., Kim, D.H., Kim, K.H., Jeon, T.Y., and Kim, D.H. (2016). Comparison Between Billroth-II with Braun and Roux-en-Y Reconstruction After Laparoscopic Distal Gastrectomy. *J. Gastrointest. Surg.* **20**, 1083–1090. <https://10.1007/s11605-016-3138-7>.
- Inokuchi, M., Kojima, K., Yamada, H., Kato, K., Hayashi, M., Motoyama, K., and Sugihara, K. (2013). Long-term outcomes of Roux-en-Y and Billroth-I reconstruction after laparoscopic distal gastrectomy. *Gastric Cancer* **16**, 67–73. <https://10.1007/s10120-012-0154-5>.
- Oizumi, K., Sekine, S., Fukagai, M., Susukida, T., and Ito, K. (2017). Identification of Bile Acids Responsible for Inhibiting the Bile Salt Export Pump, Leading to Bile Acid Accumulation and Cell Toxicity in Rat Hepatocytes. *J. Pharm. Sci.* **106**, 2412–2419. <https://10.1016/j.xphs.2017.05.017>.
- Hao, H., Cao, L., Jiang, C., Che, Y., Zhang, S., Takahashi, S., Wang, G., and Gonzalez, F.J. (2017). Farnesoid X Receptor Regulation of the NLRP3 Inflammasome Underlies Cholestasis-Associated Sepsis. *Cell Metab.* **25**, 856–867.e5. <https://10.1016/j.cmet.2017.03.007>.
- Zhao, S., Gong, Z., Zhou, J., Tian, C., Gao, Y., Xu, C., Chen, Y., Cai, W., and Wu, J. (2016). Deoxycholic Acid Triggers NLRP3 Inflammasome Activation and Aggravates DSS-Induced Colitis in Mice. *Front. Immunol.* **7**, 536. <https://10.3389/fimmu.2016.00536>.
- Takeuchi, O., and Akira, S. (2010). Pattern recognition receptors and inflammation. *Cell* **140**, 805–820. <https://10.1016/j.cell.2010.01.022>.
- Franchi, L., Eigenbrod, T., Muñoz-Planillo, R., and Núñez, G. (2009). The inflammasome: a caspase-1-activation platform that regulates immune responses and disease pathogenesis. *Nat. Immunol.* **10**, 241–247. <https://10.1038/ni.1703>.
- Lu, A., Magupalli, V.G., Ruan, J., Yin, Q., Atianand, M.K., Vos, M.R., Schröder, G.F., Fitzgerald, K.A., Wu, H., and Egelman, E.H. (2014). Unified polymerization mechanism for the assembly of ASC-dependent inflammasomes. *Cell* **156**, 1193–1206. <https://10.1016/j.cell.2014.02.008>.
- Wang, K., Sun, Q., Zhong, X., Zeng, M., Zeng, H., Shi, X., Li, Z., Wang, Y., Zhao, Q., Shao, F., and Ding, J. (2020). Structural Mechanism for GSDMD Targeting by Autoprocessed Caspases in Pyroptosis. *Cell* **180**, 941–955.e20. <https://10.1016/j.cell.2020.02.002>.
- Gros Lambert, M., and Py, B.F. (2018). Spotlight on the NLRP3 inflammasome pathway. *J. Inflamm. Res.* **11**, 359–374. <https://10.2147/jir.s141220>.
- Perera, A.P., Sajjani, K., Dickinson, J., Eri, R., and Korner, H. (2018). NLRP3 inflammasome in colitis and colitis-associated colorectal cancer. <https://10.1007/s00335-018-9783-2>.
- Chen, X., and Cubillos-Ruiz, J.R. (2021). Endoplasmic reticulum stress signals in the tumour and its microenvironment. *Nat. Rev. Cancer* **21**, 71–88. <https://10.1038/s41568-020-00312-2>.
- Lebeaupin, C., Proics, E., de Bieville, C.H.D., Rousseau, D., Bonnafous, S., Patouraux, S., Adam, G., Lavallard, V.J., Rovere, C., Le Thuc, O., et al. (2015). ER stress induces NLRP3 inflammasome activation and hepatocyte death. *Cell Death Dis.* **6**, e1879. <https://10.1038/cddis.2015.248>.
- Ren, J.L., Chen, Y., Zhang, L.S., Zhang, Y.R., Liu, S.M., Yu, Y.R., Jia, M.Z., Tang, C.S., Qi, Y.F., and Lu, W.W. (2021). Intermedin(1–53) attenuates atherosclerotic plaque vulnerability by inhibiting CHOP-mediated apoptosis and inflammasome in macrophages. *Cell Death Dis.* **12**, 436. <https://10.1038/s41419-021-03712-w>.
- Osowski, C.M., Hara, T., O’Sullivan-Murphy, B., Kanekura, K., Lu, S., Hara, M., Ishigaki, S., Zhu, L.J., Hayashi, E., Hui, S.T., et al. (2012). Thioredoxin-interacting protein mediates ER stress-induced  $\beta$  cell death through initiation of the inflammasome. *Cell Metab.* **16**, 265–273. <https://10.1016/j.cmet.2012.07.005>.
- Yuan, X., Zheng, Y., Chen, C., and Wang, C. (2017). Anisodamine inhibits endoplasmic reticulum stress-associated TXNIP/NLRP3 inflammasome activation in rhabdomyolysis-induced acute kidney injury. *Apoptosis* **22**, 1524–1531. <https://10.1007/s10495-017-1414-y>.
- Abais, J.M., Xia, M., Zhang, Y., Boini, K.M., and Li, P.L. (2015). Redox regulation of NLRP3 inflammasomes: ROS as trigger or effector? *Antioxid. Redox Signal.* **22**, 1111–1129. <https://10.1089/ars.2014.5994>.
- Lefebvre, P., Cariou, B., Lien, F., Kuipers, F., and Staels, B. (2009). Role of bile acids and bile acid receptors in metabolic regulation. *Physiol. Rev.* **89**, 147–191. <https://10.1152/physrev.00010.2008>.
- Ding, L., Yang, L., Wang, Z., and Huang, W. (2015). Bile acid nuclear receptor FXR and digestive system diseases. *Acta Pharm. Sin. B* **5**, 135–144. <https://10.1016/j.apsb.2015.01.004>.
- Mudaliar, S., Henry, R.R., Sanyal, A.J., Morrow, L., Marschall, H.U., Kipnes, M., Adorini, L., Sciacca, C.I., Clopton, P., Castellon, E., et al. (2013). Efficacy and safety of the farnesoid X receptor agonist obeticholic acid in patients with type 2 diabetes and nonalcoholic fatty liver disease. *Gastroenterology* **145**, 574–582.e1. <https://10.1053/j.gastro.2013.05.042>.
- Nevens, F., Andreone, P., Mazzella, G., Strasser, S.I., Bowlus, C., Invernizzi, P., Drenth, J.P.H., Pockros, P.J., Regula, J., Beuers, U., et al. (2016). A Placebo-Controlled Trial of Obeticholic Acid in Primary Biliary Cholangitis. *N. Engl. J. Med.* **375**, 631–643. <https://10.1056/NEJMoa1509840>.
- Younossi, Z.M., Ratziu, V., Loomba, R., Rinella, M., Anstee, Q.M., Goodman, Z., Bedossa, P., Geier, A., Beckebaum, S., Newsome, P.N., et al. (2019). Obeticholic acid for the treatment of non-alcoholic steatohepatitis: interim analysis from a multicentre, randomised, placebo-controlled phase 3 trial. *Lancet* **394**, 2184–2196. [https://10.1016/s0140-6736\(19\)33041-7](https://10.1016/s0140-6736(19)33041-7).
- Yu, J.H., Zheng, J.B., Qi, J., Yang, K., Wu, Y.H., Wang, K., Wang, C.B., and Sun, X.J. (2019). Bile acids promote gastric intestinal metaplasia by upregulating CDX2 and MUC2 expression via the FXR/NF- $\kappa$ B signalling pathway. *Int. J. Oncol.* **54**, 879–892. <https://10.3892/ijo.2019.4692>.
- Lian, F., Xing, X., Yuan, G., Schäfer, C., Rauser, S., Walch, A., Röcken, C., Ebeling, M., Wright, M.B., Schmid, R.M., et al. (2011). Farnesoid X receptor protects human and murine gastric epithelial cells against inflammation-induced damage. *Biochem. J.* **438**, 315–323. <https://10.1042/bj20102096>.
- Zhang, Z., Zou, Y.Y., Zhou, Y., Zhou, H., and Li, Y.J. (2009). The aggravatory effect of nicotine on Helicobacter pylori-induced gastric mucosa injury: role of asymmetric dimethylarginine. *J. Clin. Gastroenterol.* **43**, 261–266. <https://10.1097/MCG.0b013e3181624485>.
- Zeisel, M.B., Dhawan, P., and Baumert, T.F. (2019). Tight junction proteins in gastrointestinal and liver disease. *Gut* **68**, 547–561. <https://10.1136/gutjnl-2018-316906>.
- Cheng, Y.C., Chu, L.W., Chen, J.Y., Hsieh, S.L., Chang, Y.C., Dai, Z.K., and Wu, B.N. (2020). Loganin Attenuates High Glucose-Induced Schwann Cells Pyroptosis by Inhibiting ROS Generation and NLRP3 Inflammasome Activation. *Cells* **9**, 1948. <https://10.3390/cells9091948>.
- Cheng, S.B., Nakashima, A., Huber, W.J., Davis, S., Banerjee, S., Huang, Z., Saito, S., Sadovsky, Y., and Sharma, S. (2019). Pyroptosis is a critical inflammatory pathway in the placenta from early onset preeclampsia and in human trophoblasts exposed to hypoxia and endoplasmic reticulum stressors. *Cell Death Dis.* **10**, 927. <https://10.1038/s41419-019-2162-4>.

32. Huang, D., Xiong, M., Xu, X., Wu, X., Xu, J., Cai, X., Lu, L., and Zhou, H. (2020). Bile acids elevated by high-fat feeding induce endoplasmic reticulum stress in intestinal stem cells and contribute to mucosal barrier damage. *Biochem. Biophys. Res. Commun.* 529, 289–295. <https://doi.org/10.1016/j.bbrc.2020.05.226>.
33. Han, C.Y., Rho, H.S., Kim, A., Kim, T.H., Jang, K., Jun, D.W., Kim, J.W., Kim, B., and Kim, S.G. (2018). FXR Inhibits Endoplasmic Reticulum Stress-Induced NLRP3 Inflammasome in Hepatocytes and Ameliorates Liver Injury. *Cell Rep.* 24, 2985–2999. <https://doi.org/10.1016/j.celrep.2018.07.068>.
34. Ma, F., Ma, Y., Cui, L., Zhao, X., Wang, B., Xue, L., Wang, H., and Tian, Y. (2020). Development and characterization of a mouse model of duodenogastric reflux. *Life Sci.* 260, 118412. <https://doi.org/10.1016/j.lfs.2020.118412>.
35. Kwon, I.G., Cho, I., Choi, Y.Y., Hyung, W.J., Kim, C.B., and Noh, S.H. (2015). Risk factors for complications during surgical treatment of remnant gastric cancer. *Gastric Cancer* 18, 390–396. <https://doi.org/10.1007/s10120-014-0369-8>.
36. Fukuhara, K., Osugi, H., Takada, N., Takemura, M., Lee, S., Taguchi, S., Kaneko, M., Tanaka, Y., Fujiwara, Y., Nishizawa, S., and Kinoshita, H. (2004). Correlation between duodenogastric reflux and remnant gastritis after distal gastrectomy. *Hepato-Gastroenterology* 51, 1241–1244.
37. Miwa, K., Fujimura, T., Hasegawa, H., Kosaka, T., Miyata, R., Miyazaki, I., and Hattori, T. (1992). Is bile or are pancreaticoduodenal secretions related to gastric carcinogenesis in rats with reflux through the pylorus? *J. Cancer Res. Clin. Oncol.* 118, 570–574. <https://doi.org/10.1007/bf01211798>.
38. He, Y., Hara, H., and Núñez, G. (2016). Mechanism and Regulation of NLRP3 Inflammasome Activation. *Trends Biochem. Sci.* 41, 1012–1021. <https://doi.org/10.1016/j.tibs.2016.09.002>.
39. Lian, D.W., Xu, Y.F., Ren, W.K., Fu, L.J., Chen, F.J., Tang, L.Y., Zhuang, H.L., Cao, H.Y., and Huang, P. (2018). Unraveling the Novel Protective Effect of Patchouli Alcohol Against Helicobacter pylori-Induced Gastritis: Insights Into the Molecular Mechanism *in vitro* and *in vivo*. *Front. Pharmacol.* 9, 1347. <https://doi.org/10.3389/fphar.2018.01347>.
40. Ng, G.Z., Menheniott, T.R., Every, A.L., Stent, A., Judd, L.M., Chionh, Y.T., Dhar, P., Komen, J.C., Giraud, A.S., Wang, T.C., et al. (2016). The MUC1 mucin protects against Helicobacter pylori pathogenesis in mice by regulation of the NLRP3 inflammasome. *Gut* 65, 1087–1099. <https://doi.org/10.1136/gutjnl-2014-307175>.
41. Abu El Maaty, M.A., and Wölfl, S. (2017). Vitamin D as a Novel Regulator of Tumor Metabolism: Insights on Potential Mechanisms and Implications for Anti-Cancer Therapy. *Int. J. Mol. Sci.* 18, 2184. <https://doi.org/10.3390/ijms18102184>.
42. Shi, J., Zhao, Y., Wang, K., Shi, X., Wang, Y., Huang, H., Zhuang, Y., Cai, T., Wang, F., and Shao, F. (2015). Cleavage of GSDMD by inflammatory caspases determines pyroptotic cell death. *Nature* 526, 660–665. <https://doi.org/10.1038/nature15514>.
43. Sun, L., Cai, J., and Gonzalez, F.J. (2021). The role of farnesoid X receptor in metabolic diseases, and gastrointestinal and liver cancer. *Nat. Rev. Gastroenterol. Hepatol.* 18, 335–347. <https://doi.org/10.1038/s41575-020-00404-2>.
44. D'Amato, D., De Vincentis, A., Malinverno, F., Viganò, M., Alvaro, D., Pompili, M., Picciotto, A., Palitti, V.P., Russello, M., Storato, S., et al. (2021). Real-world experience with obeticholic acid in patients with primary biliary cholangitis. *JHEP Rep.* 3, 100248. <https://doi.org/10.1016/j.jhepr.2021.100248>.
45. Kowdley, K.V., Luketic, V., Chapman, R., Hirschfield, G.M., Poupon, R., Schramm, C., Vincent, C., Rust, C., Parés, A., Mason, A., et al. (2018). A randomized trial of obeticholic acid monotherapy in patients with primary biliary cholangitis. *Hepatology* 67, 1890–1902. <https://doi.org/10.1002/hep.29569>.
46. Song, M., Rabkin, C.S., Torres, J., Kemp, T.J., Zabaleta, J., Pinto, L.A., Hildesheim, A., Sánchez-Figueroa, L., Guarner, J., Herrera-Goepfert, R., et al. (2019). Circulating inflammation-related markers and advanced gastric premalignant lesions. *J. Gastroenterol. Hepatol.* 34, 852–856. <https://doi.org/10.1111/jgh.14518>.
47. Fang, S., Suh, J.M., Reilly, S.M., Yu, E., Osborn, O., Lackey, D., Yoshihara, E., Perino, A., Jacinto, S., Lukashcheva, Y., et al. (2015). Intestinal FXR agonism promotes adipose tissue browning and reduces obesity and insulin resistance. *Nat. Med.* 21, 159–165. <https://doi.org/10.1038/nm.3760>.
48. Lou, L.X., Geng, B., Yu, F., Zhang, J., Pan, C.S., Chen, L., Qi, Y.F., Ke, Y., Wang, X., and Tang, C.S. (2006). Endoplasmic reticulum stress response is involved in the pathogenesis of stress induced gastric lesions in rats. *Life Sci.* 79, 1856–1864. <https://doi.org/10.1016/j.lfs.2006.06.022>.
49. Wen, X., Su, B., Gao, M., Chen, J., Zhou, D., You, H., Li, N., Chang, S., Cheng, X., Qian, C., et al. (2021). Obesity-associated up-regulation of lipocalin 2 protects gastric mucosa cells from apoptotic cell death by reducing endoplasmic reticulum stress. *Cell Death Dis.* 12, 221. <https://doi.org/10.1038/s41419-021-03512-2>.
50. Chen, P., Shen, Y., Shi, H., Ma, X., Lin, B., Xiao, T., Wu, F., Zhu, J., Li, Z., Xiao, J., et al. (2016). Gastroprotective effects of Kangfuxin-against ethanol-induced gastric ulcer via attenuating oxidative stress and ER stress in mice. *Chem. Biol. Interact.* 260, 75–83. <https://doi.org/10.1016/j.cbi.2016.10.021>.
51. Baird, M., Woon Ang, P., Clark, I., Bishop, D., Oshima, M., Cook, M.C., Hemmings, C., Takeishi, S., Worthley, D., Boussiotas, A., et al. (2013). The unfolded protein response is activated in Helicobacter-induced gastric carcinogenesis in a non-cell autonomous manner. *Lab. Invest.* 93, 112–122. <https://doi.org/10.1038/labinvest.2012.131>.
52. Xiong, X., Wang, X., Lu, Y., Wang, E., Zhang, Z., Yang, J., Zhang, H., and Li, X. (2014). Hepatic steatosis exacerbated by endoplasmic reticulum stress-mediated downregulation of FXR in aging mice. *J. Hepatol.* 60, 847–854. <https://doi.org/10.1016/j.jhep.2013.12.003>.
53. Liu, X., Guo, G.L., Kong, B., Hilburn, D.B., Hubchak, S.C., Park, S., LeCuyer, B., Hsieh, A., Wang, L., Fang, D., and Green, R.M. (2018). Farnesoid X receptor signaling activates the hepatic X-box binding protein 1 pathway *in vitro* and in mice. *Hepatology* 68, 304–316. <https://doi.org/10.1002/hep.29815>.
54. Kim, D.H., Park, J.S., Choi, H.I., Kim, C.S., Bae, E.H., Ma, S.K., and Kim, S.W. (2021). The critical role of FXR is associated with the regulation of autophagy and apoptosis in the progression of AKI to CKD. *Cell Death Dis.* 12, 320. <https://doi.org/10.1038/s41419-021-03620-z>.
55. Lee, C.G., Kim, Y.W., Kim, E.H., Meng, Z., Huang, W., Hwang, S.J., and Kim, S.G. (2012). Farnesoid X receptor protects hepatocytes from injury by repressing miR-199a-3p, which increases levels of LKB1. *Gastroenterology* 142, 1206–1217.e7. <https://doi.org/10.1053/j.gastro.2012.01.007>.
56. Schneider, C.A., Rasband, W.S., and Eliceiri, K.W. (2012). NIH Image to ImageJ: 25 years of image analysis. *Nat. Methods* 9, 671–675. <https://doi.org/10.1038/nmeth.2089>.
57. Mahurkar-Joshi, S., Rankin, C.R., Videlock, E.J., Soroosh, A., Verma, A., Khandadash, A., Iliopoulos, D., Pothoulakis, C., Mayer, E.A., and Chang, L. (2021). The Colonic Mucosal MicroRNAs, MicroRNA-219a-5p, and MicroRNA-338-3p Are Downregulated in Irritable Bowel Syndrome and Are Associated With Barrier Function and MAPK Signaling. *Gastroenterology* 160, 2409–2422.e19. <https://doi.org/10.1053/j.gastro.2021.02.040>.
58. Tang, L., Tang, B., Lei, Y., Yang, M., Wang, S., Hu, S., Xie, Z., Liu, Y., Vlodavsky, I., and Yang, S. (2021). Helicobacter pylori-Induced Heparanase Promotes H. pylori Colonization and Gastritis. *Front. Immunol.* 12, 675747. <https://doi.org/10.3389/fimmu.2021.675747>.
59. Yu, J., Liu, D., Sun, X., Yang, K., Yao, J., Cheng, C., Wang, C., and Zheng, J. (2019). CDX2 inhibits the proliferation and tumor formation of colon cancer cells by suppressing Wnt/beta-catenin signaling via transactivation of GSK-3beta and Axin2 expression. *Cell Death Dis.* 10, 26. <https://doi.org/10.1038/s41419-018-1263-9>.
60. Li, S., Ma, Y.M., Zheng, P.S., and Zhang, P. (2018). GDF15 promotes the proliferation of cervical cancer cells by phosphorylating AKT1 and Erk1/2 through the receptor ErbB2. *J. Exp. Clin. Cancer Res.* 37, 80. <https://doi.org/10.1186/s13046-018-0744-0>.

**STAR★METHODS**

**KEY RESOURCES TABLE**

REAGENT or RESOURCE	SOURCE	IDENTIFIER
<b>Antibodies</b>		
Mouse monoclonal antibody GAPDH	Santa Cruz	Cat#sc-47724
Mouse monoclonal antibody FXR	Santa Cruz	Cat#sc-25309
Rabbit monoclonal antibody ZO-1	Abcam	Cat#ab276131
Rabbit monoclonal antibody occluding	Abcam	Cat#ab216327
Rabbit monoclonal antibody claudin-5	Abcam	Cat#ab131259
Rabbit monoclonal antibody TXNIP	Abcam	Cat#ab188865
Rabbit monoclonal antibody NLRP3	Abcam	Cat#ab263899
Rabbit monoclonal antibody ASC	Cell Signaling Technology	Ca#13833
Rabbit monoclonal antibody ASC	Cell Signaling Technology	Ca#67824
Rabbit monoclonal antibody Caspase-1	Abcam	Cat#ab179515
Rabbit monoclonal antibody IL-1 $\beta$	Abcam	Cat#ab254360
Rabbit monoclonal antibody IL-18	Abcam	Cat#ab243091
Rabbit monoclonal antibody IL-18	Abcam	Cat#ab207323
Rabbit monoclonal antibody GSDMD	Abcam	Cat#ab219800
Rabbit polyclonal antibody p-PERK	Invitrogen	Cat#PA5-40294
Rabbit polyclonal antibody p-eIF2 $\alpha$	Cell Signaling Technology	Cat#3398
Rabbit polyclonal antibody eIF2 $\alpha$	Cell Signaling Technology	Cat#5324
Mouse monoclonal antibody CHOP	Cell Signaling Technology	Cat#2895
Rabbit polyclonal antibody GRP78	Cell Signaling Technology	Cat#3177
Rabbit polyclonal antibody ATF6	Cell Signaling Technology	Cat#65880
Rabbit polyclonal antibody XBP1	Cell Signaling Technology	Cat#40435
Rabbit polyclonal antibody p-IRE1	Abcam	Cat#ab48187
Rabbit polyclonal antibody IRE1	Cell Signaling Technology	Cat#3294
Rabbit polyclonal antibody IgG	Abcam	Cat#ab172730
<b>Bacterial and virus strains</b>		
shGSDMD lentivirus	GeneChem biology company	N/A
shPERK lentivirus	GeneChem biology company	N/A
shCHOP lentivirus	GeneChem biology company	N/A
shFXR lentivirus	GeneChem biology company	N/A
FXR-GFP lentivirus	GeneChem biology company	N/A
<b>Chemicals, peptides, and recombinant proteins</b>		
DCA	Sigma	83-44-3
Phorbol 12-myristate 13-acetate	Sigma	16561-29-8
OCA	SELLECK	459789-99-2
CY-09	SELLECK	1073612-91-5
Triton X-100	Sigma	9036-19-5
bovine serum albumin	Sigma	9048-46-8
DAPI	Invitrogen	D1306

(Continued on next page)

**Continued**

REAGENT or RESOURCE	SOURCE	IDENTIFIER
<b>Critical commercial assays</b>		
CytoTox96 LDH-release kit	Promega	G1780
QuantiCyto Human IL-1 $\beta$ ELISA kit	NeoBioscience	EHC002bQT.48
QuickCyto Mouse IL-1 $\beta$ ELISA kit	NeoBioscience	EMC001bQT.96
QuickCyto Mouse IL-6 ELISA kit	NeoBioscience	EMC004QT.48
QuickCyto Mouse TNF- $\alpha$ ELISA kit	NeoBioscience	EMC102aQT.48
MILLICELL-ERS	Millipore	MERS00002
CellTiter-Glo luminescent cell viability assay	Promega	G7570
CCK-8 assay	MedChemExpress	HY-K0301
<b>Experimental models: Cell lines</b>		
GES-1 cells	SIBCB	N/A
RAW 264.7 cells	SIBCB	N/A
U-937 cells	SIBCB	N/A
<b>Experimental models: Organisms/strains</b>		
C57BL/6	SLACCAS	N/A
<b>Software and algorithms</b>		
Prism Graphpad 7.0	GraphPad Software	<a href="https://www.graphpad.com/">https://www.graphpad.com/</a>
ImageJ	Schneider et al. <sup>56</sup>	<a href="https://imagej.nih.gov/ij/">https://imagej.nih.gov/ij/</a>

**RESOURCE AVAILABILITY****Lead contact**

Further information and requests for resources and reagents should be directed to and will be fulfilled by the Lead Contact, Xuejun Sun ([sunxy@mail.xjtu.edu.cn](mailto:sunxy@mail.xjtu.edu.cn)).

**Materials availability**

The lentivirus are available upon request. This study did not generate other unique reagents.

**Data and code availability**

- Data reported in this paper will be shared by the [lead contact](#) upon request.
- The sequencing data generated in this study are deposited to the NCBI SRA repository (<http://submit.ncbi.nlm.nih.gov/subs/sra/SUB14168407>) and are publicly available
- Any additional information required to reanalyze the data reported in this paper is available from the [lead contact](#) upon request.

**EXPERIMENTAL MODEL AND STUDY PARTICIPANT DETAILS****Cell cultures**

Normal human and rat gastric epithelial cells (GES-1 and RGM-1) and mouse macrophage cell line RAW 264.7 cells were all routinely cultured in DMEM supplemented with 10% fetal bovine serum (FBS) at 5% CO<sub>2</sub> at 37°C. Human monocyte cell lines U-937 were maintained in RPMI supplemented with 10% FBS. U-937 monocytes were differentiated into macrophages by stimulating with 50 nM PMA (Phorbol 12-myristate 13-acetate, Sigma Aldrich) for 24 h and used for further experiments. Once the cells reached 70% confluence, they were treated with 100  $\mu$ M DCA for different hours. All the cells were purchased from Shanghai Institute of Cell Biology, Chinese Academy of Sciences.

**Animal model of DGR**

All animal experiments were performed in accordance with the institutional guidelines, and were approved by the Laboratory Animal Center of Xi'an Jiaotong University. The male C57BL/6 mice were purchased from Shanghai SLAC Laboratory Animal Co., Ltd. (Shanghai, China). The mice were randomly assigned to two groups according to the different surgical procedure. Mice in the control group (n = 8) did not undergo surgery. Mice in the gastrojejunostomy (GJ) group (n = 24) underwent side-to-side GJ without gastrectomy. This was performed between the greater curvature of the glandular stomach and the jejunum, 2 cm distal to the ligament of Treitz, to mimic Billroth II gastrectomy in humans.

Twelve hours before surgery, the mice were deprived of food and orally administered polyethylene glycol solution for bowel preparation. The surgery was performed in accordance with a standardized protocol. The mice had access to tap water and solid food immediately after surgery. They were sacrificed at 2, 4, and 8 weeks after surgery (8 mice each time in GJ group). Thereafter, the intragastric contents and gastric tissues around the GJ were collected. For drug interventions, the nude mice were randomly divided into four subgroups and were administered by oral gavage of OCA (10, 20 mg/kg/day) alone or in combination with intraperitoneal injection of 20 mg/kg/day NLRP3 inhibitor CY-09 for every one day for 8 weeks.

## METHOD DETAILS

### Lentiviral vectors and transfection

Lentiviral vectors with GSDMD/PERK/CHOP/FXR shRNA or FXR overexpression were constructed and prepared by GeneChem Co., Ltd. (Shanghai, China). All transfections were performed according to the manufacturer's instructions.

### CCK-8 assay

For CCK-8 assay, cells were seeded into 96-well culture plates at 3000 cells/well for 48 h. Cell viability was checked by CCK-8 assay according to manufacturer's protocol. Normalization was done to cells treated with DMSO as vehicle, which were defined as 100%.

### LDH, IL-1 $\beta$ , IL-6, and TNF- $\alpha$ release assay

LDH, IL-1 $\beta$ , IL-6, and TNF- $\alpha$  were measured using a CytoTox96 LDH-release kit (Promega, Madison, WI, USA) and a QuantiCyto IL-1 $\beta$ , IL-6 or TNF- $\alpha$  ELISA kit (Neobioscience, Chenzhen, China) according to the manufacturer's instructions. The absorbance value at 450 nm was then measured. Each experiment was repeated three times.

### Measurement of Trans-epithelial electrical resistance (TER)

The resistance across the stratified epithelium was measured using MILLICELL-ERS (Millipore Corporation, Bedford, MA, USA) with 'chopstick' electrodes according to a previously described method.<sup>57</sup> The value obtained from a blank insert was subtracted to give the net resistance, which was multiplied by the membrane area to give the resistance in area-corrected units ( $\Omega \cdot \text{cm}^2$ ).

When resistance was stable (at  $>1500 \Omega \cdot \text{cm}^2$ ), the culture medium from the upper (apical) compartment of the monolayer was removed and replaced with a medium containing acid (pH 2–4) or control medium. Cell viability was evaluated using the CellTiter-Glo luminescent cell viability assay (Promega, Madison, WI, USA) according to the manufacturer's instructions. Each experiment was performed in triplicate.

### Histopathological analysis

One set of sections was stained with hematoxylin and eosin (H&E) and examined under a microscope. All stained sections were reviewed by two blinded consultant histopathologists. The degrees of mucosal inflammation were graded on the basis of previously delineated criteria.<sup>58</sup>

### Total protein extraction and western blotting

The detailed protocol was performed as described previously.<sup>59</sup> The antibody information was presented in the section of [key resources table](#). Each experiment was performed in triplicate.

### RNA isolation and real-time PCR

RNA isolation, complementary DNA (cDNA) synthesized and real-time PCR were performed as described previously.<sup>59</sup> The sequences of primers were summarized in [Table S1](#). Each experiment was performed in triplicate.

### RNA-sequencing

The RNA-sequencing was performed on BGISEQ-500 by BGI company (Shenzhen, China). The data were analyzed on Dr. Tom Multi-Omics Data Mining System (<https://biosys.bgi.com/>).

### Immunofluorescence (IF)

The cells were fixed with 4% paraformaldehyde for 20 min and permeabilized with 0.2% Triton X-100 for 10 min. After blocking with 5% bovine serum albumin (BSA) for 30 min at room temperature, the cells were incubated at 4°C overnight with primary antibodies against NLRP3 (1:100 dilution). The dishes were washed three times with PBS for 10 min each and then incubated with Alexa Fluor 488-conjugated secondary antibodies (1:400 dilution, Invitrogen, Carlsbad, CA, USA) for 1 h at room temperature. The nuclei were stained with DAPI (10 mg/mL) for 10 min. The samples were examined via microscopy (Leica Microsystems, Heidelberg, Germany) to analyze NLRP3 staining.



### **Immunoprecipitation (IP) assay**

The cells were washed three times with ice-cold PBS and harvested at 4°C in immunoprecipitation lysis buffer. Co-IP assay was then performed as described previously.<sup>60</sup> Each experiment was performed in triplicate.

### **Statistical analysis**

The differences among the groups were compared by the Student's *t* test or one-way ANOVA. All statistical analyses were performed using the SPSS statistical package (SPSS Inc., Chicago, IL, USA).  $p < 0.05$  was considered statistically significant.